High Efficiency CIGSS Thin Film based Solar Cells and Mini-modules

Ahmed Ennaoui*
University Mohammed V,
Physics Department, Faculty of Sciences, BP 1014 Rabat-Morocco

The highest efficiency for $Cu(Ga,In)Se_2$ (CIGS) thin-film-based solar cells has been achieved with CdS buffer layers prepared by a solution growth method known as the chemical bath deposition (CBD). With the aim of developing Cd-free chalcopyrite-based-thin-film solar cells, we describe the basic concepts involved in the CBD technique. The recipes developed in our laboratory for the heterogeneous deposition for good-quality thin films of ZnO, ZnSe, ZnS are presented. In view of device optimization, the initial formation of chemical-bath-deposited ZnSe thin films on $Cu(Ga,In)(S,Se)_2$ (CIGSS) and the subsequent development of the CIGSS/ZnSe heterojunction were investigated by X-ray photoelectron spectroscopy (XPS). The good surface coverage was controlled by measuring changes in the valence-band electronic structure as well as change in the In_{4d}, Zn_{3d} core lines. From these measurements, the growth rate was found to be around 3.6 nm/min. The valence band and the conduction band-offsets ΔE_V and ΔE_C between the layers were determined to be 0.60 and 1.27 eV, respectively for the CIGSS/ZnSe interface. The energy band diagram is discussed in connection with the band-offsets determined from XPS data. Small and large area CIGSS based solar cells with a CIGSS/Zn(Se,OH)/ZnO structure are produced. A ZnSe thickness below 10 nm has been found to be optimum for achieving a homogeneous and compact buffer layer on CIGSS with an active area efficiency of 15.7%. Using Siemens Solar technology this structure is adapted to fabricate Cd-free CIGSS monolithic mini-modules with efficiencies up to 11.7%.

I. INTRODUCTION

CIGSS/CdS devices - $CuInSe_2$ (CIS), or if gallium is added, also $Cu(In,Ga)Se_2$ (CIGS) has reached the highest efficiencies of all thin film cells. The record laboratory efficiency recently announced by National Renewable Energy Laboratory (NREL, USA) is around 18.8% [1]. Very recently Angstrom Solar Center (Uppsala Sweden) presented new world record for CIGS based mini-modules of 16.6% [2]. The heterojunction partner materials in CIS and CIGS solar cells are as critical as the absorber itself in determining the performance of the cell. The old junction model of CdS/CIS solar cells was a p-n heterojunction between n-type CdS and p-type CIS. Euro-CIS groups carefully analyzed the CdS/CIS interface by photoemission spectroscopy and they proposed a model of a $CuIn_3Se_5$/CIS heterojunction between n-type $CuIn_3Se_5$ and p-type CIS [3]. The CdS films used for high efficiency CIS solar cells have been deposited by chemical bath deposition process. CdS layers deposited by physical vapour deposition do not show a high efficiency. It was said that the CBD is a soft process and CdS films can cover a rough CIS surface with less damage to the absorber surface than the PVD process does. Furthermore the oxide layer can be removed from the CIGS surface by CBD- process and the high quality p-n junction can be formed.

NREL-group studied the interaction between the CBD process and the CIGS surface [4]. They reported that the Cd^{2+} solution modified the CIGS surface favorably. They pointed out that during the CBD process, Cd substituted CIGS is formed resulting in an n-type region. Then the CdS film grows slowly as sulfur is slowly released by the hydrolysis of thiourea. Furthermore an intermixing at the CdS/CIGS interface involving S, Se, and In has been identified and the formation of various interlayers is assumed [5].

Cd-free CIGS devices - It is highly desirable to replace CdS by a less toxic alternative buffer layer. Zn-compounds such as Zn(S,OH) and Zn(Se,OH) deposited by CBD process are promising candidates and have achieved efficiencies up to 15% [6-16]. In the present study we report on a chemical bath process for the deposition of Zn-compounds buffer layers. For device optimization production-scale $Cu(In,Ga)(SeS)_2$ (CIGSS) were subjected to different alkaline baths containing $ZnSO_4$ with two complexing agents (NH_3, NH_2NH_2) and two chalcogen precursors $XC(NH_2)_2$ (X = Se,S). After different deposition times the CIGSS/Zn(Se,OH) interface was investigated by XPS and SEM. Furthermore, XPS-UPS method was used for studying the CIGSS/Zn(Se,OH) heterojunction formation and directly determining the valence-band offsets. Theoretical progress in attaining a comprehensive understanding of the band discontinuities is reviewed. The photovoltaic performance of CIGSS/Zn(X,OH) thin film solar cells and mini-modules are reported. Our Cd-free solar cells efficiencies are certified by the Frauenhofer Institute for Solar Energy Systems.

II. EXPERIMENTAL PROCEDURE

A. CHEMICAL BATH DEPOSITION

The chemical bath method requires the presence of reagents that act as a source of chalcogen ions and complexion of the metal ion of interest. The CBD process involves a heterogenous growth mechanism

E-mail: Ennaoui@fsr.ac.ma

(film formation) that competes with homogeneous precipitation. The first mechanism can proceed either by "ion by ion" or "cluster by cluster" and gives adherent mirror-like compact films. The second mechanism gives poorly adherent, powder-like porous films. However, the stability equilibrium of metal provides a concentration of the cation small enough to produce the controlled homogeneous precipitation of the film on a solid substrate. The presence of metal hydroxide in the deposition bath is unvoidable due to the aqueous alkaline nature of the chemical bath. This results in the formation Zn(O,OH), Zn(Se,OH), Zn(S,OH), rather than ZnO, ZnSe, ZnS, respectively [17-19]. The inclusion of hydroxide ions was observed in the CBD-CdS as well [20].

ZnX, Zn(X,OH) with X = S,Se - The metal precursor $ZnSO_4$ solution (0.4M/l) and two different ligands hydrazine NH_2NH_2 and ammonia NH_3 were mixed under constant stirring. The resulting solution (A) was turbid milky due to the formation of $Zn(OH)_2$. Excess of NH_3 was added to bind most of $Zn(OH)_2$ as a complex ion. In order to decrease the free metal ion concentration, the ratio of ammonia to hydrazine hydrate in this solution was carefully adjusted. The chalcogenide source $XC(NH_2)_2$ (solution B) consists of $SeC(NH_2)_2$ ($8x10^{-2}$ M/l) in an alkaline bath or $SC(NH_2)_2$ ($4x10^{-2}$ M/l). The following conditions were used to produce high quality devices: Solution (A) is heated to T_{sub}. Next the CIGSS substrates are immersed, for few minutes. Then the solution B containing $SeC(NH_2)_2$ or $SC(NH_2)_2$ is added. The flow chart of the growth mechanism for $Zn(OH)_2$, ZnX and Zn(X,OH) is shown in Fig. 1. The concentration of hydroxide OH^- must be low enough so that hydrolysis of $XC(NH_2)_2$ to take place mostly at the surface as follow:

$$XC(NH_2)_2 + OH^- \rightarrow HX^- + CH_2N_2 + H_2O \quad (1)$$

$$HX^- + OH^- \rightarrow X^{2-} + H_2O \quad (2)$$

This ensures that the ionic product $[Zn^{2+}]$ $[X^{2-}]$ in the bulk of the bath is less than the solubility product of ZnX.

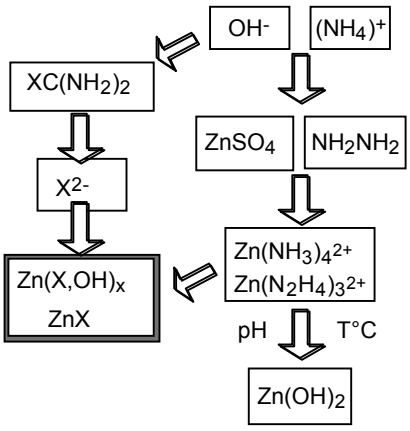

FIG. 1: Flow chart of growth mechanism for CBD-ZnX and Zn(X,OH) (X = S, Se)

ZnO and Zn(O,OH) - 0.5 M $ZnSO_4$, ammonia, and distilled water at room temperature were mixed in a beaker and stirred continuously. The reaction mixture was adjusted to pH 11. Two methods are used for the preparation of ZnO. In the first method the substrate is immersed in an alkaline (pH 11) ammoniacal bath heated at 65°C. The second method is based on successive ion layer adsorption and reaction (SILAR) [17,21] and involves three steps: (i) specific adsorption of zinc amine solution by substrate immersion in a solution containing $Zn(NH_3)_4^{2+}$ at room temperature, (ii) introduction of the substrate in hot water at T = 95°C, and (iii) water rinsing in order to remove ZnO particles. This last method allowed a layer by layer heterogenous growth mechanism. Oxygen may be supplied by adsorption of hydroxyl anion, which leads to the formation of ZnO.

B. DEVICE PREPARATION

The state-of-the-art base line CIGS-based device structures are based on a CIGS absorber layer and a ZnO transparent top window which are separated by a thin CdS buffer layer

CIGSS -absorbers – At Siemens Solar, $Cu(Ga,In)(S,Se)_2$ (CIGSS) samples were synthesized by rapid thermal processing (RTP) of elemental Cu, In(Ga)-Se stacked layers on DC-magnetron sputtered Mo-coated Na-lime glass [22]. The deposition process is split into two steps: coating of the elements at room temperature, followed by annealing. CIGSS Layers produced by this process contain no Ga near the surface.

Moderate substrate temperature (below 550°C) was used to avoid substrate bending.

Single cells and mini-modules - CIGSS based thin-film solar cells were fabricated with two interface structures: CIGSS/Zn(Se,OH) and CIGSS/Zn(Se,OH).

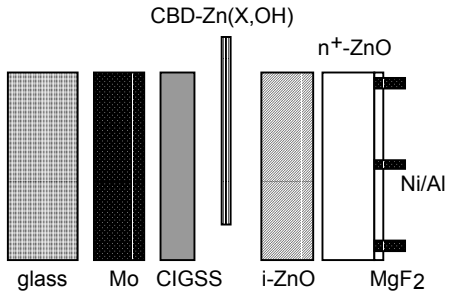

FIG. 2a : Schematic representation of a CIGSS-based single cell device.

When these devices are measured as single cells (see Fig. 2a), the device structures were completed by the standard procedure of When these devices are measured as single cells (see Fig. 2a), the device structures were completed by the standard procedure of depositing ZnO by RF sputtering in two layers: a high-resistivity layer of undoped ZnO in a partial pressure of O_2 to a thickness of 110 nm and a conductive layer of Al or Ga-doped ZnO to a thickness of 400 nm. Next, Ni/Al finger grids were

deposited by e-gun evaporation through a shadow mask followed by a 120 nm MgF_2 antireflection coating.
When the CIGSS substrates are used for minimodules production, compatible coating and patterning techniques are used such as ZnO metal organic chemical vapor deposition (MOCVD) or DC-sputtering from ceramic targets, dip coating, laser and mechanical scribing [23].

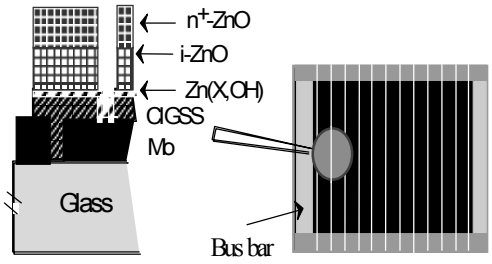

FIG. 2b: Structure and appearance of patterned Cd-free CIGSS mini-module on a 5 x 10 cm^2 substrate

The appearance of a mini-module circuit structure is schematically shown in Fig. 2b. Cells are interconnected monolithically, as shown in the inset.

III. EXPERIMENTAL RESULTS

A. GROWTH KINETICS

Ex-situ photoemission spectra were performed before and after each growth step in order to observe the evolution of the electronic structure of the CIGSS/Zn(Se,OH) heterojunction. X-ray photoemission spectra of Zn_{3d} and In_{4d} core levels were recorded using the Mg K_α line (1253.6 eV). The samples were transfered to the UHV system (a commercial multi-technique surface science system VG-ESCALAB; base pressure: 10^{-10}mbar) as fast as possible in order to minimize contamination. In Fig. 3 we plot the XPS region of Zn_{3d} core-level emission. The CIGSS coverage is indicated for different buffer layer thickness. The deconvoluted Zn_{3d} peaks show two doublets. The more pronounced peak is located at 10.1 eV up to 1.8 nm Zn(Se,OH) coverage and shifts to 9.8 eV for 3.6 nm, 7.2 nm and 10.8 nm thick Zn(Se,OH) buffer layers.

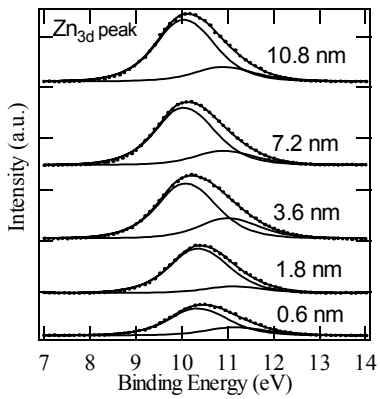

FIG. 3: Zn_{3d} core level emission with increasing Zn(Se,OH) coverage of CIGSS substrates

We attribute this peak to Zn(Se,OH). The second peak at higher binding energy is attributed to Zn(OH). The In_{4d} peak is attenuated with increasing Zn(Se,OH) coverage (see Fig. 4).

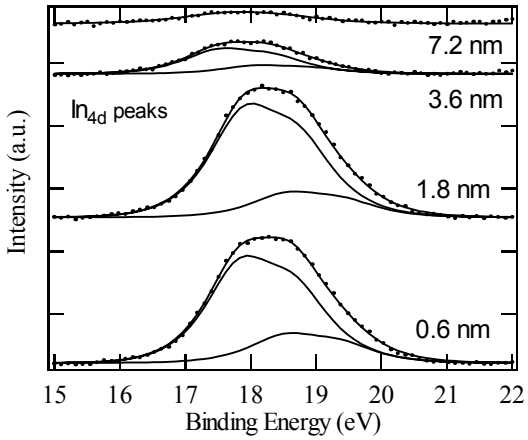

FIG. 4: In_{4d} core level emission with increasing Zn(Se,OH) coverage of CIGSS substrates

A Zn(Se,OH) thickness below 10 nm is obtained for conformal coverage of the absorber. In order to obtain good quality buffer layers, the homogeneous precipitation of metal ions and their inclusion in the films must be minimized The precipitating agents are provided by the hydrolysis of $SeC(NH_2)_2$ and by the formation of Zn(OH). The control of precipitation of chalcogenides and hydroxide is possible by using N_2H_4 and NH_3.

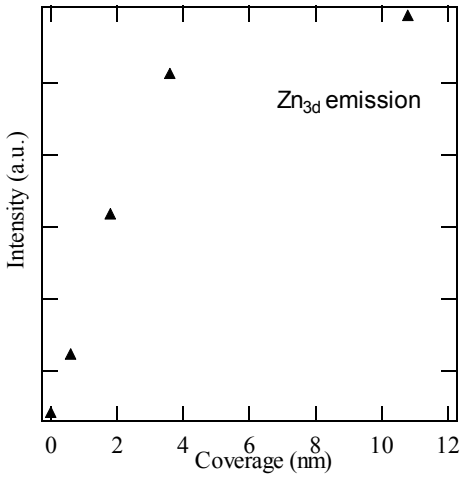

FIG. 5: Evolution of the Zn_{3d} intensity with increasing Zn(Se,OH) coverage

The use of NH_3 and N_2H_4 separately leads to little or no growth. The film growth is observed when both NH_3 and N_2H_4 are used [16].

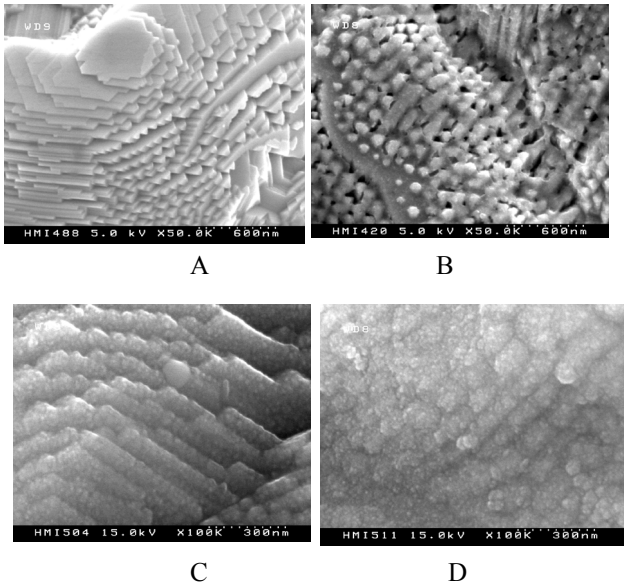

FIG. 6 : Zn(Se,OH) on CIGSS as revealed by SEM for different deposition times: (A) CIGSS surface, (B) t = 20, (C) t = 3 min, (D) t = 12 min.

The pronouced Zn_{3d} signal increases lineary with increasing Zn(Se,OH) coverage up to 67s of deposition time (Fig. 5). Further prolonged deposition time yields only a small increase in the Zn_{3d} signal.
This self-limiting process has the advantage of yielding a good surface coverage at a minimum thickness. This result is supported by the planar view of the scanning electron micrographs of CIGSS and Zn(Se,OH) coated CIGSS for different deposition times (see Fig. 6). The micrograph for the virgin CIGSS surface (Fig. 6A) is used as reference. The growth of Zn(Se,OH) particles in lateral direction can be observed in Fig 6B after 20s deposition time. A small change in the shape of CIGSS crystallites can be seen. Small Zn(Se,OH) nuclei are grown on CIGSS facets which are not completely covered yet. We believe that the driving force for such two dimensional growth can be understood by the similarity of the Zn(Se,OH) and CIGSS lattice constants. Once the surface is covered laterally with Zn(Se,OH) nuclei (Fig. 6C), the three dimensional growth of Zn(Se,OH) takes place (see Fig. 6D). Fig. 6C shows the two dimensional growth, the Zn(Se,OH) particles are grown in size. Their elongated shapes cover the whole surface.

B. BAND LINE-UP

The valence band and conduction band offsets ΔE_V and ΔE_C for the system CIGSS/ Zn(Se,OH) are determined by measuring the binding energies ΔE_{In4d} of In_{4d} in CIGSS and $\Delta E_{Zn_{3d}}$ of Zn3d in $Zn(Se,OH)_x$ with respect to the valence band maximum (VBM). An ultraviolet source was used to determine this maximum from the valence band spectra during the heterojunction formation. Furthemore a Shirley-type background was subtracted prior to peak fitting with Gaussian-Lorentzian profile. The spin-orbite splitting of In_{4d} and Zn_{3d} peaks were determined with high accuracy using ultra-violet photoelectron spectroscopy (UPS). ΔE_V and ΔE_C are given by:

$$\Delta E_V = \Delta E_{In4d} - \Delta E_{Zn3d} - \Delta E_{CL} \quad (3)$$

$$\Delta E_C = \Delta E_V - E_G \text{ (absorber)} + E_G \text{ (buffer)} \quad (4)$$

The In_{4d} peak position for CIGSS is found to be ΔE_{In4d} = 17.1 eV while for Zn(Se,OH) we have taken ΔE_{Zn3d} = 8.8 eV, which is the peak position where the emission from the substrate has disappeared completely. The average energy difference between the Zn3d and In4d levels, where both substrate and buffer layer emissions are present at 0.6 nm, 1.8 nm, 3.6 nm and 7.2 nm effective Zn(Se,OH) coverages is found to be ΔE_{CL} = 7.70 eV.

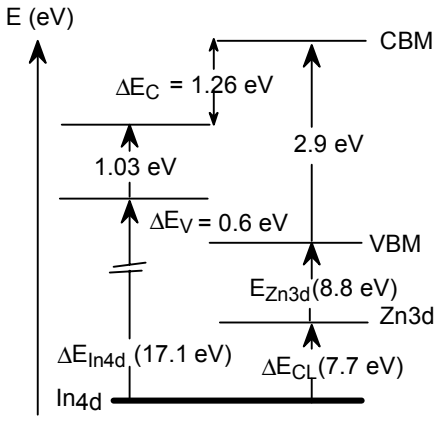

FIG. 7: Schematic energy-level diagram of $Cu(In,Ga)(S,Se)_2$ heterojunction. The experimentally determined core-level energies with respect to valence-band maxima as well as the difference between core-level binding energies (ΔE_{CL}) are given.

The optical band gaps for CIGSS absorber and Zn(Se,OH) buffer layer are E_G(absorber) = 1.03 eV and E_G (buffer) = 2.9 eV respectively.

Table I: Measured valence-band discontinuity
$^{S-C}$: Single crystal. $^{T-E}$: Thermal evaporation. ^{Cal}:Calculated. ^{Mes}:Mesured. ^{CBD}:Chemical bath deposition. ^{MBE}:Molecular beam epitaxy. CIGSS: Siemens absorber

Devices	ΔE_V	Ref.
$^{S-C}CuInSe_2/^{T-E}CdS$	0.8 eV	[24]
$^{S-C}CuInSe_2/^{T-E}ZnSe$	0.7 eV^{mes} 0.6 eV^{cal}	[25]
$CuInSe_2$/CdS $CuInSe_2$/ZnSe	1.07 eV ^{Cal} 0.7 eV ^{Cal}	[26]
CIGSS/^{CBD}ZnSe	0.6 eV	This work
CIGSS/^{MBE}ZnSe	0.5 eV	[27]

Using the relations (3) and (4) one may determine the valence band and the conduction band offsets to be ΔE_V = 0.6 eV and ΔE_C = 1.27 eV. These results are schematically summarized in Fig. 7. The valence-band offsets determined in this work are compared to those obtained by several authors (see Table I)

C. DEVICE PERFORMANCE

Current voltage (J-V) characterization is carried out at AM1.5 illumination, and device efficiencies are quoted as total area to include grid losses.

Table II : PV-parameters of CIGSS devices under AM1.5 condition. S_1 and M_1 are confirmed by FhG/ISE. [a]Total area with ARC, [b]Active area, [c]Total area without ARC
M: Samples from Siemens Germany. S: Samples from Siemens California.

cell	Buffer	Area cm^2	V_{OC} mV	I_{SC} mA cm^{-2}	FF %	Eff. %
S1	Zn(Se,OH)	0.537	535.08	36.1	70.7	13.67[a]
M1	Zn(Se,OH)	1.08	565.74	35.95	70.9	13.26[a] (15.7[b])
M2	Zn(Se,OH)	0.6	570	36.6	69	14.2[c]
M3	Zn(S,OH)	0.475	569.4	34.9	71	14.2[c]

The cell performances were tested at the Frauenhofer Institute for Solar Energy Systems (FhG-ISE-Freiburg-Germany). The PV parameters are summarized in Table II. Best temperatures for the deposition of Zn(Se,OH) buffer layers are found to be T = 70°C.

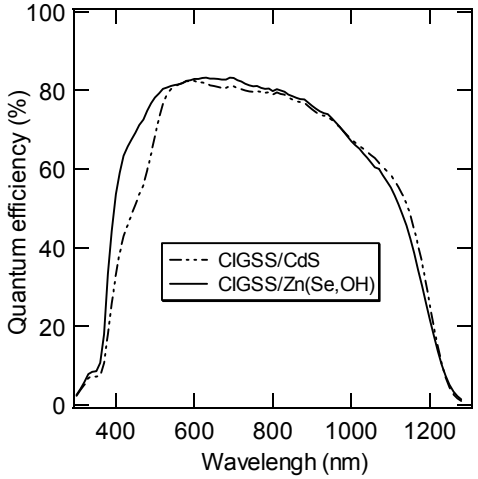

FIG. 8 : Quantum efficiency of 13.7% efficient CIGSS/Zn (Se,OH) based solar cell compared to a 13.1% CIGSS/CdS standard device

The CIGSS/Zn(Se,OH)/ZnO device exhibits an improved fill factor (FF). Comparable efficiency was achieved at lower temperature for the CIGS/Zn(S,OH)/ZnO system. For this device high open circuit voltage was obtained at T_{sub} = 50°C [9]. For comparaison, a cell based on the same CIGSS absorber with a standard CBD-CdS Buffer layer had a total area effieciency of 13.1% with open-circuit photovoltage V_{OC} = 545 mV, short-circuit photocurrent density J_{SC} = 33.0 mA cm^{-2}, and fill factor FF = 73%). All cells show the phenomenon known as light soaking. The efficiencies shows a relative increase by up to 5% after 30 min light exposure (AM1.5 under open circuit conditions). In Fig 8 we compare the quantum efficiency of cell S_1 (see table II) with the (13.1%) cell prepared with the standard CBD-CdS buffer layer. The spectral response rises around 1200 nm. Both cells reach a maximum quantum efficiency at around 85%. A significantly enhanced blue response of the cell with Zn(Se,OH) is observed.

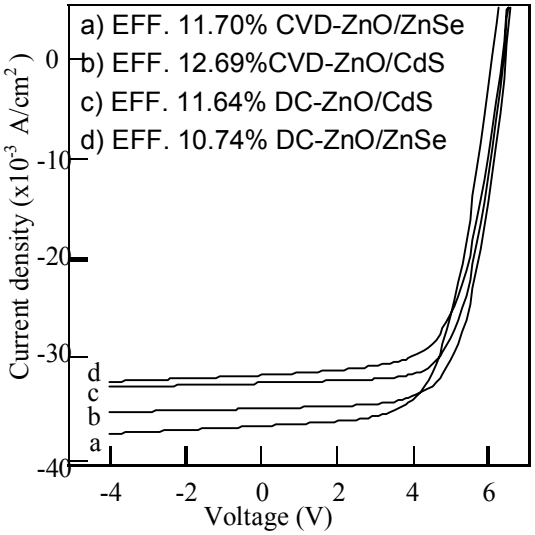

FIG. 9: J-V characteristics of CIGSS based mini-modules with 20 cm^2 aperture area with have 12 interconnected cells (a) and (d) and 11 interconnected cells (b) and (c)

Considerable progress is made by combinning CIGSS absorbers with dip coated Zn(Se,OH) and Zn(S,OH) for the preparation of CIGSS based minimodule using Siemens technology. (see Fig. 2b). As shown in Fig. 9 and table III efficiencies up to 11.7% were found with Zn(Se,OH) buffer layers while the efficiency of the CdS-buffered reference mini-module is around 13%.

Table III. PV parameters of CIGSS/CdS and CIGSS/ZnSe Based minimodules with 11 interconnected cells and 12 interconnected cells respectively (data from Fig. 9)

ZnO process	Buffer layer	V_{OC} mV	I_{SC} $mAcm^{-2}$	FF %	Eff.
MOCVD	CdS	5926.03	34.58	68.1	12.68
DC-sput.	CdS	6385.73	32.20	67.9	11.64
MOCVD	ZnSe	6091.25	36.47	63.1	11.70
DC-sput.	ZnSe	6352.59	31.40	64.6	10.74

IV. SUMMARY

We have shown that the combination of production-scale CIGSS absorber fabricated by Siemens

Solar and chemically deposited Zn-compounds buffer layers made it possible to achieve high efficiencies of 15.7% (active area) and over 14% (total area). The CBD process has proved to be a successful means of delivering an ultra-thin buffer layer of Zn(Se,OH) between the absorber and the ZnO window. The determination of the band alignment between Zn(Se,OH) and $Cu(In,Ga)(SeS)_2$ using X-ray photoelectron spectroscopiy has been presented. Zn(Se,OH) films with increasing thickness were stepwise deposited in a chemical bath on $Cu(In,Ga)(SeS)_2$ surface. The valence band offset of $Cu(In,Ga)(SeS)_2$/Zn(Se,OH) is found to be (0.6 ± 0.1) eV. Minimodules (circa 20 cm^2 aperture area) using Zn(Se,OH) buffer layers and 12 interconnected monolithic cells shows an efficiency of 11.7%.

V. CRITICAL DISCUSSION

A. CURRENT THEORETICAL APPROCHES

The above results are unexpected as the conduction band edge discontinuity for Zn(Se,OH) is significantly high. Basically the transport properties of all heterojunction devices strongly depend on three interfaces characteristics [28]: band discontinuities, interface states, and potential-barrier height (see Fig. 10). The change in the forbidden gap across the interface is distributed between ΔE_V and ΔE_C. These discontinuities may form barriers for the charge carrieres crossing the interface and dramatically influence the operation of the heterojunction devices. Interface states, including defect states, also influence theheterojunction-device behavior by acting as charge traps or recombination centers. Finally, the position of E_F at the interface determine the barrier height on the two sides of the interfaces, V_{D1} and V_{D2}. Different theoretical models are developed to calculate the valence-band discontinuity for any heterojunction interface. The Anderson´s electron-affinity rule theory [29], is based on the free-surface properties of the two semiconductors. ΔE_C is given by the difference between the electron affinities of the two semiconductors.

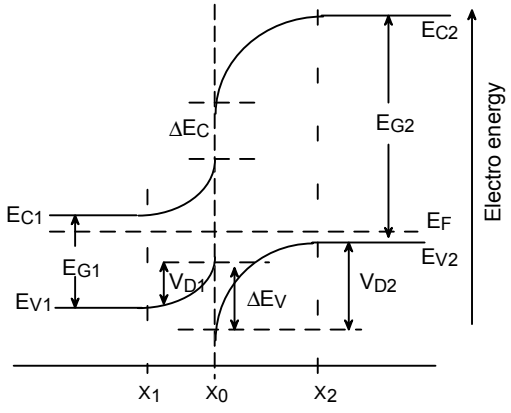

FIG. 10: Schematic energy-band diagram for a semiconductor-semiconductor interface. The two semiconductors have bad gaps E_{G1} and E_{G2}. The difference between the two gaps gives rise to a conduction-band discontinuity, ΔE_C, and to a valence-band discontinuity, ΔE_C.

This model is very widely used in hetrojunction-device research. Harrison [30], used a tight-binding approch to calculate the absolute position of the valence-band maximum (VBM). Frensley and Kroemer [31], used a pseudopotential approch to calculate the valence-band maximum relative to an average interstitial potential. Adam and Nussbaum [32], calculated the valence-band discontinuity by aligning the intrinsic Fermi levels of the two semicinductors. Von Ross [33], estimated ΔE_C to be zero, thus ΔE_V is equal to the difference between the forbidden gaps. All these models tried to calculate the band-line-up from bulk crystal properties. Another approach is based on the local electronic structure of the interface e.g. self-consistent theory of Baraff [34], Pickett [35]. Cluster approach of Swart [36]. All the above models ignore the peculiar microscopic properties of each interface such as interdiffusion during the heterojunction formation, formation of chemical bonds. These phenomena can affect the charge distribution on each side of the interface and therefore the band discontinuity. A realistic band discontinuity model should take all these effects into consideration.

B. CURRENT EXPERIMENTAL APPROACH

New analytical tools using synchrotron-radiation photo-emission have now given direct evidence for the intermixing of the constituent elements at the CIGSS/CdS interface [5]. Combination of X-ray emission spectroscopy (XES) and X-ray photoelectron spectroscopy using high brightness synchrotron radiation was employed to investigate electronic and chemical structure of the buried CIGS/CdS interface. Direct evidence of diffusion of sulfur from the CdS into the absorber and out-diffusion of In into the CdS over a depth of less than 50 nm. There is no evidence for a pure CdS layer (see Fig. 10). Very recently we observed a strong intermixing between absorber, buffer and TCO material in the interface region using X-ray photoelectron spectroscopy XPS and elastic recoil detection analysis (ERDA) [37]. We should conclude that in chalcopyrite devices [38], the surface chemistry is closely linked to device performance.

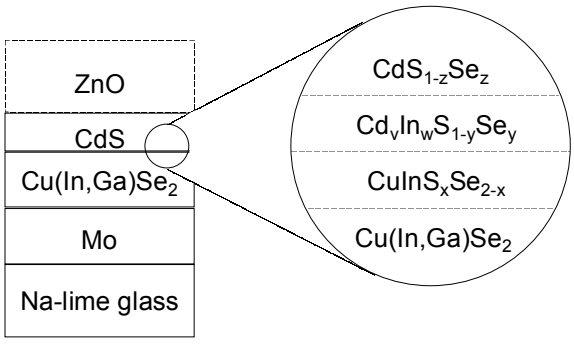

FIG. 11: Schematic diagram of the CdS/CIGS interface based on XES/PES analysis after [5]

Although the exact mechanism for junction formation is not clearly understood, several models based on experimental results could explain how the junction is formed: (i) XPS-UPS identification of an ordered vacancy compound (OVC) with a band gap of about 1.3 eV which lead to a buried $CuInSe_2$/OVC/CdS (or ZnS) heterojunction [3]. This OVC layer is a Se vacancies and/or a Cu-poor region and contain $CuIn_3Se_5$ and/or $CuIn_5Se_8$ (ii) PL measurements and SIMS analysis of Cd (or Zn) doping of CIGS during the CBD-process [39,40]. It is believed that the surface reaction with Cd^{2+} (or Zn^{2+}) ions resulted in an n-type region forming a buried junction. The following substitution reaction was reported:

$$Cd^{2+} + Cu(In,Ga)Se_2 \rightarrow Cd_xCu_{1-2x}(In,Ga)Se_2 + 2xCu^{2+} \quad (5)$$

Furthermore it was reported that $CuIn_3Se_5$ phase is more easy doped than the $CuInSe_2$ [39].

(iii) Microscopic interaction of Na with, e.g.defects, Se, or oxygen impureties [41]. Na affect the texture and physical properties of chalcopyrite absorbers. It increases the electrical conductivity, reduces the space charge width and improves the photovoltage.

VI. FINAL REMARKS

A. FUTURE R&D EFFORT

Production line of CIGSS/CdS technology is presently under construction and intense R&D work is going on by Siemens in California (USA) and Munich (Germany). Current CIGSS-products from Siemens Solar (ST series) are available as 5, 10, 20, and 40 W modules [42,43]. The record efficiency measured by Siemens are 12.1% for large commercial size modules and 14.7% for small laboratory module [44]. In the last European Photovoltaic Solar Energy conference Angström Solar Center (Uppsala University) presented efficiencies over 16% for large area minimodules. The ZSW center (Zentrum für Sonnenenergie- und Wasserstoff-Forschung, Germany) started a pilot production of 1.2 MWp/year capacity in 1999 at Würth Solar (Germany) and a CIGS-production line with 10MWp/year is planned. The know-how for the preparation of CIGS-absorbers (one-step thermal evaporation)[45], was initially developed at the IPE (Institut of Physical Electronic, University of Stuttgard, Germany). The results were transferred to an industrial scale at ZSW.

Substantial progress to replace Cd-containing buffer layers has been achieved during the last few years. In the 11th PVSEC-11 (International Photovoltaique Energy Conference, Hokkaido 1999) Showa Shell (Japan) [11], presented efficiency over 11% for large area Cd-free CIGS/Zn(O,S,OH) based mini-module and the following aggressive goals have been targeted: 13% efficiency on a 30 x 30 cm^2 and development of fabrication technologies to achieve 140 yen/Wp at annual production capacity of 100 MWp/a by the end of FY2000. As can be seen in the discussions the surface, interface and process integration issues play a key role in the transition from an R&D type process to a pilot production or even manufacturing line. The next R&D subject are: (i) determination of the degree of interdiffusion and ion-exchange. (ii) possible formations of lower band gap phases can be a key for understanding the role of the buffer layer. (iii) increase in the efficiency over 15% on large Modules to compete practically with crystalline Si power modules for utility application.

B. COSTS OF CIGSS TECHNOLOGY

Thin film technology is very promising because the cost of manufacturing the circuit should be much lower for thin films than it is for crystalline silicon. A cost of \$1 per W_p was calculated by Siemens Solar for a 24-MW_p base line CIGSS process factory operating on 350 days/year [46]. The product 2 x 4 foot module (12% efficiency) and the package was glass/EVA/glass laminated. The total cost of a $Cu(In,Ga)(SeS)_2$ module is estimated to be about \$120/m^2, substatially lower than the most favorable projections for crystalline silicon.

ACKNOWLEDGEMENTS

We would like to acknowledge the support of the extended HMI teams especially I. Sieber for SEM. This work was in part supported by the European Commission within the framwork of the Joule III project “Wide band gap CPV” under contract no. JOR3-CT97-0135. Siemens Solar GmbH was supported by the European Union under the framework of the Joule III program (Project CT97-0129).

[1] J.R. Tuttle, M.A. Contreras,T.J. Gillespie, K.R. Ramanathan, A.L. Tennant, J. Keane, A.M. Gabor and R. Noufi, Progress in Photovotaic 33 (1999), p. 235.

[2] J. Kessler, M. Bodegard, J. Hedstrom, and L. Stolt, 16th European Photovoltaic Solar Energy Conference, Glasgow, May 2000.

[3] D. Schmid, M. Ruckh, F. Grunwald and H.W. Schock J. Appl. Phys. 73 (1993) 2902

[4] K.R. Ramanathan, H: Wiesner, S: Asher, D. Niles, N. Bhattacharya, J. Keane, M.A. Contreras, and R. Noufi, Proceeding of the 2nd World Conference and Exhibition on Photovoltaic Solar Energy Conversion. Vol. 1 (1998) pp. 477-481

[5] C. Heske, D. Eich, R. Fink, E. Umbach, T. van Buuren, C. Bostedt, L.J. Terminello, S. Kakar, M.M. Grush, T.A. Callcott, F.J. Himpsel, D.L. Ederer, W. Riedl, F. Karg, Appl. Phys. Lett Vol. 74 (1999) p. 1451

[6] A. Ennaoui, Can. J. Phys. 77 (1999) p. 723

[7] A. Ennaoui, U. Blieske, M. Ch. Lux-Steiner, Progress in Photovoltaics 6 (1999) p. 447.

[8] A. Ennaoui, M. Weber, M. Saad, W. Harneit, M. Ch. Lux-Steiner, F. Karg, Thin Solid Films 361-362 (2000) p. 450.
[9] A. Ennaoui, M. Lux-Steiner and F. Karg. 11th. International Photovoltaic Science and Engineering Conference, September 20-24 (1999), Technical Digest, p. 79, Hokkaido, Japan.
[10] T. Nakada, K. Furumi; M. Mizutani, Y. Hagiwara and A. Kunioka, 11th International Photovoltaic Science and Engineering Conference, September 20-24 (1999), Technical Digest, p. 81, Hokkaido, Japan.
[11] K. Kushiya, M. Tachiyuki, Y. Nagoya, A. Fujimaki, 11th International Photovoltaic Science and Engineering Conference, September 20-24 (1999), Technical Digest, p. 637, Hokkaido, Japan.
[12] Y. Ohtake, T. Okamoto, A. Yamada, M. Konagai, K. Saito, Solar Energy Material and Solar Cells (Special volume PVSEC-9) 49, 269 (1997)
[13] K. Kushiya, M. Tachiyuki, T. Kase, , I. Sugiyama, Y. Nagoya, D. Okumura, M. Sato, O. Yamase, H. Takeshita, Solar Energy Material and Solar Cells (Special volume PVSEC-9), 49 277 (1997).
[14] F. Cooray, K. Kushiya, A. Fujimaki, I Sugiyama, T. Miura, D. Okumura, M. Sto, M. Ooshita, O. Yamase Solar Energy Material and Solar Cells (Special volume PVSEC-9) 49, 291 (1997).
[15] J.M. Dona, J. Herrero, J. Electrochem. Soc. 142, 764 (1995)
[16] I.O Oladeji, L. Chow Thin Solid Films 339, (1999) 148
[17] A. Ennaoui, M. Weber, C.D. Lokhande, R. Scheer, H.J. Lewerenz. Solar Energy Mater. Sol. Cells, 55 (1998) p. 277
[18] C.D. Lokhande, P.S. Patil, A. Ennaoui, H. Tributsch. Solar Energy Mater. Sol. Cells, 55 (1998) p. 379
[19] A. Ennaoui, C.D. Lokhande, M. Weber, R. Scheer, H.J. Lewerenz. Proceeding of the 2nd Word Conference on Photovoltaic Solar Energy Conversion, Vienna, Austria. (1998) p. 628
[20] R. Ortega-Borges and D. Lincot. J. Electrochem. Soc. 140 (1993) p.3464
[21] A.E. Jimenez-Gonzailer and P.K. Nair. Semicon. Sci. Technol. 10 (1995) p. 1277
[22] F. Karg, V. Probst, H. Harems, G. Rimmasch, W. Riedl, J. Kotschy, J. Holtz, R. Treichler, O. Eibl, A. Mitwalsky, A. Riendl, Proc. 23rd. IEEE Photovoltaic Specialist Conf. (1993) p. 441.
[23] A. Ennaoui, W. Eisele, M. Ch. Lux-Steiner, F. Karg, W. Riedl, 16th European Photovoltaic Solar Energy Conference, Glasgow, May 2000.
[24] T. Löher, W. Jaegermann, C. Pettenkoffer, J. Appl. Phys. 77 (1995) p. 731
[25] A. J. Nelson, C.R. Schwerdtfeger, su-Huai, and A. Zunger, Appl. Phys. Lett. 62 (1993) p. 2557
[26] Su-Huai Wei and A. Zunger, Appl. Phys. Lett. 63 (1993) p. 2549
[27] M. Wörz, E. Pschorr-Schoberer, R. Flierl, H. Preis, and W. Gebhardt, J. Appl. Phys. 84 (1998) p.2871.
[28] A:L: Fahrenbruch and J: Aranovich, edited by B.O. Seraphin, Solar Energy Conversion – Solid state aspect. Topic in Applied Physics Vol.31, Springer-Verlag, Berlin, Heidelberg,New York 1979)
[29] R. Anderson, Solid State Electron. 5 (1962) 341.
[30] W. Harrison. J. Vac. Sci. Technol. 14 (1977) 1016
[31] W.R. Frensley and H: Kroemer, Phys. Rev. B 15 (1977) 2642.
[32] M.J. Adam and Allen Nussbaum, Solid State Electron. 22 (1979) 783.
[33] Oldwig Von Ross, Solid State Electron. 23 (1980) 1069.
[34] G.A. Baraff, Joel A. Appelbaum, and D.R. Hamann, Phys. Rev. Lett. 38, (1977) p. 237
[35] W. Pickett, S.G. Louis, and M.Cohen, Phys. Rev. Lett. 39 (1977)p.109; Phys. Rev. B 17 (1978) p. 815
[36] C. A. Swart, W.A. Goddard, and T.G. McGill, J. Vac. Technol. 19, (1981) p. 551
[37] I. Luck, U. Störkel, W. Bohne, A. Ennaoui, M. Schmidt, H.-W. Schock and D. Bräunig, E-MRS Spring Conference, Thin Film Chalcogenide Photovoltaic Materials, May 30 – June 2nd (2000)
[38] M. Lux-Steiner, A. Ennaoui, Ch.-H. Fiescher, A. Jäger-Waldau, J. Klaer, R. Klenk, R. Könenkamp, Th. Matthes, R. Scheer, S. Siebentritt, A. Weidinge, Thin Solid Films 361-362 (2000)p. 533, and references therein.
[39] T. Wada, S. Hayashi, Y. Hashimoto, S. Nishiwaki, T. Sato, T. Negami, and M. Nishitami, 2nd Word Conference on Photovoltaic Solar Energy Conversion, Vienna, Austria. (1998) p. 403
[40] I. Luck, A. Ennaoui, D. Bräunig, A. Antonia, E. Terzini, M. Schmidt, and H. W. Schock, 16th European Photovoltaic Solar Energy Conference, Glasgow, May 2000.
[41] M. Ruckh, D. Schmid, A. Kaiser, R. Schaffler, T. Walter, and H. W. Schock, Solar Energy Mater. And Solar Cells, 41/42 (1996) p. 335.
[43] R. Gay, M. Dietrich, C. Freric, C. Jensen, K. Knapp, D. Tarrant, D. Willet, 12th European Photovoltaic solar energy conference, (1994) p. 935.
[42] Siemens Solar Press Relese, Camarillo, CA (September 29th, 1998);
e-mail: http://www.solarpv.com/0328.htm
[44] F. Karg. 11th. International Photovoltaic Science and Engineering Conference, September 20-24 (1999), Technical Digest, p. 627, Hokkaido, Japan.
[45] W.H. Bloss, Proc. 1st World Conf. Photovoltaic Energy Conversion, Hawaii, IEEE, New York (1994) p. 15
[46] K.E. Knapp, C. Eberspacher, D. Tarrant, and G. Pollock, 23rd IEEE Photovoltaic specialist conference, Louisville. May 1993. P. 1073